Nano Research

Open Access

Research Article

Scalable fabrication of ultrahigh-conductivity SWCNT films via a redispersion method for photovoltaic/thermoelectric coupling systems

Xiaoyang Yuan[1,2], Dehua Yang[1,2,3] ✉, Xiaofei Yang[1,2], Xuan Chang[1,2], Donghui Zhang[1,2], Aiai Wang[1,2], Yiming Xu[1,2], Xueliang Yang[1], Jingxin Chen[3], Xuejian Li[3], Shuai Ma[3], Qing Gao[1,2,3], Shufang Wang[2], Huaping Liu[4], and Jianhui Chen[1,2,3] ✉

[1] *Advanced Passivation Technology Lab, College of Physics Science and Technology, Hebei University, Baoding 071002, China*
[2] *Province-Ministry Co-Construction Collaborative Innovation Center of Hebei Photovoltaic Technology, College of Physics Science and Technology, Hebei University, Baoding 071002, China*
[3] *State Key Laboratory of Photovoltaic Materials and Cells, Yingli Group Co., Ltd, Baoding 071051, China*
[4] *Beijing National Laboratory for Condensed Matter Physics, Institute of Physics, Chinese Academy of Sciences, Beijing 100190, China*

Cite this article: *Nano Research*, **2025**, *18*, 94907383. https://doi.org/10.26599/NR.2025.94907383

ABSTRACT: Photovoltaic/thermoelectric (PV/TE) coupling systems simultaneously cool solar cells and recover waste heat. Single-wall carbon nanotubes (SWCNTs) films are expected to simultaneously exhibit their electrical conductivity, thermal conductivity, and thermoelectric properties in this application. Fabricating SWCNTs films with polymer-dispersed SWCNTs are simple, safe, and scalable. However, the difficulty in simultaneously enhancing both dispersion quality and SWCNT concentration significantly limit the electrical conductivity of these films. Herein, we develop a SWCNT redispersion method in Nafion ethanol system to achieve well-dispersion at high SWCNT concentrations. Using this dispersion, A4-sized films were readily prepared, achieving remarkable electrical conductivity of 1.97 MS/m. The large-area film exhibits a high power factor (654.37 μW/(m·K²)) and apparent thermal conductivity (529 W/(m·K)), and is integrated into a 330 cm² thermoelectric/photovoltaic coupling system. The PV output power increases by 220 mW. An additional 70 mV thermoelectric voltage is generated. Moreover, the investigation of the drying process unravels how polymer, solvent and SWCNT concentration collectively dominate the film uniformity. This work significantly enhances the electrical conductivity of polymer-dispersed SWCNTs and explores an application direction that simultaneously utilizes their high thermoelectric performance and thermal conductivity, highlighting their great application potential in PV/TE systems.

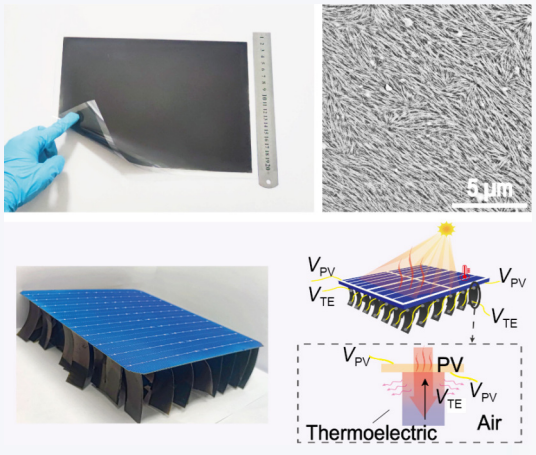

KEYWORDS: single-wall carbon nanotube, dispersion, high-conductivity films, thermoelectric, photovoltaic/thermoelectric coupling

1 Introduction

Single-wall carbon nanotubes (SWCNTs) are conceptually tubular nanostructures composed of roll-up graphene sheets [1]. The fabrication of large-area and high-quality SWCNT films is essential for SWCNT-based flexible electrodes, transparent conductors, flexible thermoelectric generators, solar cells and thin-film transistors. SWCNT thermoelectric devices are featured with flexibility, lightweight, and high power density [2]. However, SWCNT thermoelectric films face two levels of challenges: (1) Achieving high conductivity in large-area films remains challenging, especially for polymer/SWCNT composites. The power factor (PF) is defined as: $PF = S^2\sigma$, where σ and S represent electrical conductivity and Seebeck coefficient, respectively. Even with doping, which sacrifices the Seebeck coefficient, the

Received: February 11, 2025; **Revised:** March 15, 2025
Accepted: March 17, 2025

✉Address correspondence to Dehua Yang, yangdehua@hbu.edu.cn; Jianhui Chen, chenjianhui@hbu.edu.cn

conductivity remains relatively low, significantly limiting their PF [3–6]. Although high PF of > 200 μW/(m·K²) have been successfully achieved with *in-situ* polymerization or polymer-sorted semiconducting SWCNTs [5, 7], small film sizes, complex fabrication processes, and high costs significantly hinder scalability. (2) Increasing electrical conductivity often leads to increased apparent thermal conductivity [8], reaching > 400 W/(m·K²) [9–12]. And, the near-blackbody emissivity leads to great radiant heat loss [12]. Thus, the figure-of-merit (ZT) of SWCNT films for traditional thermoelectric applications is limited. Exploring optimal application scenarios that harness both the thermoelectric properties and thermal conductivity of SWCNT films may provide new insight for their thermoelectric applications.

The waste heat generated by solar cells significantly reduce their conversion efficiency [13]. The photovoltaic (PV) output of different types of solar cells decreases by 0.17%–0.5% per °C [14, 15]. Especially, the working temperature of solar cells in the field often exceeds 25 °C and can reach up to 80 °C in desert. Therefore, reducing the temperature and utilizing the waste heat through a hybrid photovoltaic/thermoelectric (PV/TE) system are of significant practical importance. Bulk TE materials such as bismuth telluride has been integrated into PV modules [15]. However, these materials are designed to have low thermal conductivity to achieve high ZT values, which hinders the heat dissipation of PV devices. The PV/TE system requires both high PF and good thermal dissipation. Integrating SWCNT TE modules into PV modules to simultaneously achieve thermoelectric conversion and solar cell cooling not only enhances PV performance but also utilizes the waste heat. Particularly, considering that the global total installed capacity of solar cells has already reached 1418 GW in 2023, a 0.1% increase in solar cell efficiency could result in an additional 1.4 GW of power, potentially opening new avenues for the application of SWCNTs.

Considering the large area of PV modules, the high-efficiency fabrication of large-area, high-performance SWCNT films is essential for PV/TE systems. Two main approaches are commonly used to prepare SWCNT films: chemical vapor deposition methods (CVD) [16] and wet-processed method [17, 18]. Compared with CVD methods, wet-processed films are readily patterned and shaped, free from the CVD reactor size limitations that restrict the width of continuously synthesized films [19, 20]. Wet processing enables the scalable preparation of uniform films with industrial coating techniques, such as blade coating and spraying [18, 21], provided the film structure remains intact during drying process. This could overcome the trade-off between yield and performance in CVD methods [22, 23].

The performance of wet-processed films depends on the SWCNT concentration in the dispersion (or SWCNT density in the conductive film), dispersion quality (the degree of dispersion) and the drying process. These factors influence the SWCNT the electrical performance, film uniformity and scalability. However, it is difficult to optimize all these factors simultaneously.

The density of conductive pathways in a film is determined by the concentration of well-dispersed SWCNTs. The increased SWCNT density in films exponentially boosts conductivity by reducing volume porosity [2]. Meanwhile, the degree of dispersion of SWCNTs is also of great importance. The junction resistance between nanotubes dominates the overall resistance of a SWCNT film [24]. Specifically, the junction resistance between bundles with diameter of 7–14 nm is approximately 20 times higher than that between individual SWCNTs [24]. However, achieving both high concentration and high dispersion quality is difficult, as the sharp rise in viscosity with increasing SWCNT concentration significantly reduces dispersion efficiency [25–27]. Despite superacid achieve high concentration of well-dispersed SWCNTs [25, 28], this scenario faces safety concern in industrial-scale film fabrication. High concentration (> 1 mg/mL) was achieved in surfactant aqueous solutions [26]. However, these dispersions encounter challenges such as dewetting and "coffee ring" effects when using industrial film-forming techniques [29, 30].

Polymer-dispersed SWCNTs are compatible with industrial film-forming techniques. The high viscosity of polymer solutions suppresses the formation of "coffee ring" [31]. Compared with small molecules, polymers also suppress the dewetting of thin film due to intensified interaction with substrates [32]. However, the major limitation of polymer-based systems is their low conductivity. The electrical conductivity of polymer-dispersed SWCNT films rarely exceeds 0.3 MS/m even after doping [33–38], which is generally lower than that achieved by CVD-grown films [39–41]. The polymers capable of dispersing SWCNTs, such as Nafion [42], poly(vinylpyrrolidone) (PVP) [43], poly(dimethylsiloxane) (PDMS) [44] and sulfonated polyetheretherketone (SPEEK) [45], are nonconductive and difficult to remove from SWCNT surfaces. In these systems, a substantial increase in SWCNT concentration/density is required to offset the adverse effects of these polymers on electrical conductivity. Conductive polymers are ether poor soluble (poly(3,4-ethylenedioxythiophene) (PEDOT)) [6], or require complex *in situ* polymerization on nanotubes (polyaniline (PANI) and polypyrrole (PPy)) [35, 36], making them less effective as dispersants. Additionally, the higher viscosity of SWCNT/polymer dispersions compared to surfactant-based ones limits sonication efficiency [46, 47], making it difficult to achieve monodisperse or thin-bundled SWCNTs at concentrations > 1 mg/mL. As a result, the polymer-dispersed SWCNT films suffer from either low SWCNT concentration or poor dispersion quality. Therefore, achieving both high concentration and excellent dispersion quality is crucial for improving electrical conductivity of polymer-dispersed SWCNT films. It is also a prerequisite for the preparation of large-area, high-performance films using industrial film-forming techniques. Among various polymers, Nafion exhibits excellent dispersion capability for SWCNTs, particularly in water and alcohols, making it a promising candidate for achieving high-concentration SWCNT dispersions. Its inability to fully disperse high-concentration SWCNTs is primarily constrained by the high viscosity of the dispersion, which reduces the efficiency of ultrasonication. We expect that a significant increase in the concentration of well-dispersed SWCNTs will substantially enhance Nafion-SWCNT film's conductivity.

This work presents an improved redispersion strategy that simultaneously enhances dispersion quality, SWCNT concentration, and large-area film uniformity. For the first time, by precisely controlling the evolution of rheological properties with ultrasonic energy input, well-dispersed SWCNTs were achieved in Nafion ethanol solutions at 3 mg/mL with viscosity > 25 Pa·s, revealing a nematic phase transition during drying. Owing to the high viscosity and shear thinning profiles, uniform thin films were readily prepared on various substrates using simple doctor blading. The conductivity of a wet-processed A4-size film reached 1.97 MS/m, which is ~ 1000 times improvement over previously

reported SWCNT-Nafion films [34, 38]. The film fabrication is simple and does not require highly precise film-forming processes and has the potential to scale film areas to arbitrary sizes. Large-area film with a high PF of 654.37 μW/(m·K^2) and apparent thermal conductivity of 529 W/(m·K) are integrated into a photovoltaic/thermoelectric system. The SWCNT film generated a 70 mV thermoelectric voltage. The conversion efficiency of solar cell improved by 0.63% via cooling. We also unraveled that the viscosity, surface tension, and drying dynamics together govern liquid-phase film quality, offering insights to suppress dewetting and coffee ring effects. Our approach demonstrates a synergistic optimization of fabrication simplicity and film performance and provides new insights for electronic and thermoelectric applications of SWCNTs.

2 Experimental methods

2.1 Dispersion of high-concentration SWCNTs

Nafion solution (25 wt.% in isopropanol, Sigma-Aldrich) was diluted to 0.5 wt.% by ethanol (> 99.5%, Sigma-Aldrich). 27 mg of raw SWCNTs (CoMoCAT, carbon > 95%, Sigma-Aldrich) (Tuball, carbon > 80%, Sigma-Aldrich) were added to 9 mL of 0.5 wt.% Nafion ethanol solution in a 20 mL vial. For traditional sonication method, the mixture was sonicated by a tip-homogenizer at 40% amplitude for 120 min. During the sonication process, the dispersion was immersed in a 15 °C water bath. The sonication instrument displays the acoustic energy delivered to the dispersion in real-time by receiving feedback from the dispersion. When the viscosity is too high, ultrasonic propagation is obstructed, and the homogenizer cannot effectively deliver acoustic energy to the dispersion. After 120 min of sonication, as gelation occurred in the dispersion, the effective acoustic energy delivered, as indicated by the instrument, no longer increased. For the present sonication method, the mixture of SWCNT and Nafion was sonicated at 40% amplitude for 45 min, followed by a mild centrifugation at 13,000 g for 10 min. The 90% supernatant was collected and redispersed in the same manner for 75 min.

2.2 Preparing large-area SWCNT films

To prepare high-conductivity SWCNT film, 25 mL of as-prepared 3 mg/mL SWCNT dispersion was dipped onto the untreated substrate (such as clean glass, PET and silicon wafers). A doctor blade with a length of 22 cm was used to prepare A4-sized films. The gap between the blade and the substrate was set to 400 μm. During the blade coating, the doctor blade pushed the dispersion at a speed of 1 cm/s to cover the entire substrate. The liquid film was dried for 3 h. The entire doctor-blading process was carried out in a cleanroom. To improve the conductivity, the film was treated with 16 mM ethanol solution of $AuCl_3$ using spraying. Finally, the carbon nanotube film was subjected to a cold pressing treatment at 3 megapascals for 20 min.

2.3 Thermoelectric performance

The thermoelectric film was obtained by cutting a 1-μm-thick SWCNT film, prepared on a PET substrate, into rectangular strips along with the substrate. The Seebeck coefficient of the TE film was measured at 25 °C under vacuum conditions using a Seebeck testing instrument (CTA-3S). A mini thermoelectric module was fabricated by connecting multiple such strips in series using copper tape and compressing them. The current–voltage and current–power curves of the thermoelectric module under different temperature gradients were measured using a LCR meter. The apparent thermal conductivity was carried out by steady-state method with IR thermometer [10]. The measurement setup was placed in an airtight and windless environment. The intrinsic thermal conductivity was measured and calculated following Zhou's method [12].

2.4 Photovoltaic/thermoelectric system

The passivated emitter and rear contact (PERC) silicon solar cell was purchased from DASOLAR. A thermocouple was attached to the back of the cell using silver paste, and the temperature changes were monitored under exposure to simulated sunlight at 10 times the standard intensity. The top and bottom of each double-sided TE film were connected using copper tape, and the films were adhered to the back of the cell and connected in series. Then, the temperature changes of the cell under illumination were recorded. Subsequently, the PV performance of the cell and the TE performance of the series-connected films were respectively measured at the corresponding temperatures.

2.5 Characterization

The morphology of SWCNTs in films were characterized by scanning electron microscopy (SEM, Nova NanoSEM450, FEI). The optical absorption and transmittance spectra were characterized by ultraviolet–visible–near-infrared (UV–vis–NIR) spectrophotometer (Lambda 950, PerkinElmer). The light path length is 10 mm when measuring dispersions. Raman spectra were obtained using a confocal Raman microscope (HR Evolution, Horiba). Resistance of SWCNT films were measured using a four-probe measurement system (tip spacing 1 mm). Thickness of SWCNT films was measured using a profilometer (Dektak XT, Bruker). The viscosity at different shear rate was measured using a rheometer (MARS 40, HAAKE). The temperature of dispersions was fixed at 25 °C during measurement. The contact angle measured was carried out using an optical contact angle system (XG-CAMA, XYCXIE). The surface tension was obtained through pendent drop apparatus (SL250, Kino), with the values provided by the software output. Polarized optical microscopy images were obtained using a microscope (bx51m, Olympus) equipped with polarizing filters. The samples for optical microscopic characterization were prepared on glass substrates.

3 Results

3.1 High-concentration well-dispersed SWCNT dispersion in polymer-ethanol solution

To increase the density of SWCNTs in films, we attempt to increase the concentration of SWCNT dispersion at a fixed concentration of Nafion using the traditional sonication method. This method, as reported in the literature, involves mixing the raw material with a dispersant in a solvent and sonicating until a stable dispersion is achieved. CoMoCAT SWCNT with a diameter range of 0.8–1.0 nm was used as the raw material. Different amounts of raw SWCNT powder were added to 9 mL of 0.5 wt.% Nafion ethanol solutions to achieve SWCNT concentrations of 0.5, 1, 2 and 3 mg/mL. The mixtures were sonicated with a tip-type homogenizer for 0.5, 1, 2 and 3 h. As shown in Fig. 1(a) and Fig. S1 in the Electronic

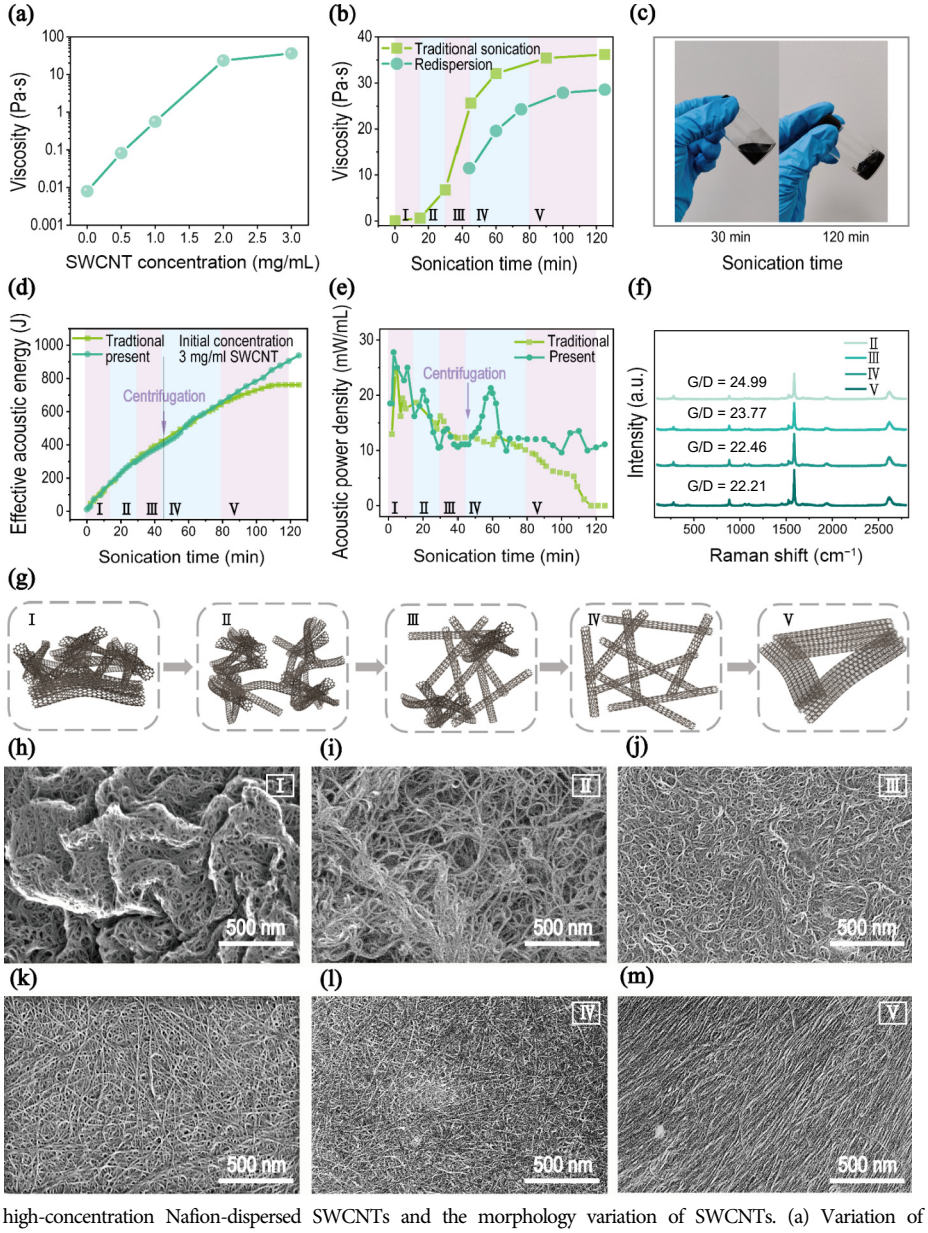

Figure 1 Preparation of high-concentration Nafion-dispersed SWCNTs and the morphology variation of SWCNTs. (a) Variation of viscosity with SWCNT concentration in dispersions prepared using traditional sonication method. The viscosity values in the panel are the viscosities measured at a shear rate of 1 s^{-1}. (b) Variation of viscosity with sonication time for 3 mg/mL dispersions prepared using the traditional and present sonication strategies. The mild centrifugation was performed at 45 min. (c) Photographs of 3 mg/mL SWCNT dispersions after sonication for 30 and 120 min using traditional sonication method. (d) Effective acoustic energy delivered to the dispersion as a function with sonication time. The different colored regions delineate the various stages of sonication. (e) Variation of acoustic power density with sonication time. The acoustic power density is derived from the derivative of the curve in (d) divided by the dispersion volume. (f) Raman spectra of the dispersions prepared by the present method at different sonication stages. (g) Schematic diagram of SWCNT films prepared from the dispersion at different sonication stages. SEM images of SWCNT films prepared from dispersions at stage (h) I, (i) II, and (j) III. (k) SEM image of SWCNT film prepared from dispersion after 120 min of sonication using traditional sonication procedure. SEM images of films prepared from dispersions at stages (l) IV and (m) V after centrifugation.

Supplementary Material (ESM), the viscosity of the dispersions increased dramatically with the SWCNT concentration. At 3 mg/mL, the dispersion became extremely viscous with increasing sonication time Fig. 1(b) and Fig. S2 in the ESM. After sonicating for 60 min, the viscosity plateaued. We hypothesize that the viscosity of the solution reached the homogenizer's limit for dispersing the SWCNT-polymer mixtures. This is reasonable considering that high viscosity significantly increases the cavitation threshold, inhibiting formation and implosion of bubbles [27]. As shown in Fig. 1(c), the 3 mg/mL dispersion fluidity decreases significantly as sonication time increases, preventing further ultrasonic processing. In a polymer system, at a given SWCNT concentration, the viscosity of the SWCNT-polymer mixture serves as an indicator for assessing dispersion quality [48]. When SWCNTs are well-dispersed at 3 mg/mL, the viscosity should be distinctly higher than that of the 2 mg/mL dispersion. Yet, Fig. 1(a) shows similar the viscosities for both, suggesting lower dispersion quality at 3 mg/mL. Hence, the traditional sonication method fails to achieve optimal dispersion at this concentration.

Thus, we employed the redispersion method, in which a mild centrifugation is performed after a long-term sonication to eliminate the impurities and large bundles followed by a second

sonication process. A schematic diagram is present in Fig. S3 in the ESM. The impurities and large bundles increase viscosity, consuming effective acoustic energy and hindering ultrasonic propagation [26]. To minimize the loss of SWCNT during centrifugation and to ensure the remaining bundles were sufficiently small for further dispersion, we employed a relatively mild centrifugation at 13,000 g for 10 min after a long-term sonication. Figure 1(b) shows a significant viscosity reduction post-centrifugation. Subsequent sonication further increased viscosity, indicating SWCNT detachment from bundles [26]. To achieve high-efficiency sonication at the highest possible viscosity, we investigated the variation of effective acoustic energy delivered to the dispersion with sonication time in Fig. 1(d) and obtained the acoustic power density via differentiation (Fig. 1(e)). The dispersion process is divided into five stages. In the current method, the mild centrifugation is performed after stage III, where both viscosity and acoustic energy increase rates slowed. The high viscosity prevents the ultrasonic propagation. It hinders the acoustic energy delivery to dispersion and results in the decrease in acoustic power density. In the traditional dispersion method, without the mild centrifugation, the delivery of effective acoustic energy to dispersions becomes progressively more difficult as sonication time increases. Eventually, the homogenizer cannot work at such high viscosity, leading to zero acoustic power density (Fig. 1(e)). The viscosity was reduced by approximately 55% after the mild centrifugation, followed by a rapid increase during further sonication until stabilizing at ~ 29 Pa·s. Meanwhile, during the redispersion process, after a brief increase at stage IV, the acoustic power density decreased and stabilized at approximately 10 mW/mL at stage V, indicating that the present method maintains good sonication efficiency, facilitating the continuously delivery of acoustic energy to SWCNTs for the detaching bundles.

Compared with the traditional sonication method, the effective acoustic energy continuously increased after centrifugation, indicating effective energy propagation (Fig. 1(d)). The corresponding increase in viscosity suggests enhanced dispersion quality with time (Fig. 1(b)). Even at 29 Pa·s (120 min), acoustic energy continued to be effectively delivered, indicating successful SWCNT dispersion at this viscosity. As viscosity plateaued in stage V, it suggests near-maximal dispersion degree under current conditions. Moreover, we detected the temperature change during sonication, as shown in Fig. S4 in the ESM. Compared with the centrifugation-redispersion strategy, the dispersion temperature was much higher when using the traditional sonication method. It suggests that the acoustic energy degraded into heat due to high viscosity [27]. Although the increased temperature reduces the viscosity of a solution, it also accelerates SWCNT reaggregation and has been demonstrated to cause poor dispersion quality [49]. Raman spectroscopy confirms that the present method does not significantly increase defects in the SWCNTs, as evidenced by the G/D ratio changes (Fig. 1(f)).

The morphological changes in SWCNTs directly reflect variations in dispersion quality (Fig. 1(g)). We prepared SWCNT film by blade coating with the dispersions at different sonication stages (Figs. 1(h)–1(m)). Initially, the SWCNTs twisted with each other in large clusters (Fig. 1(h)). As sonication time increasing, effective acoustic energy was successively delivered to crash the SWCNT clusters (Fig. 1(i)). As the SWCNTs on the surface of the bundles were stripped via cavitation effect, the bundles became thinner with the specific surface area increasing Fig. 1(j)), resulting in enhanced friction [26]. At this stage, the percolation event occurs with the improved dispersion quality. The enhanced inter-tube and tube-bundle interactions result in a distinct change in rheological behavior [50]. As a result, the viscosity was dramatically increased at stage III (Fig. 1(b)). Furthermore, the polymers' backbones act as cross-linkers for forming the three-dimensional gel networks with well-dispersed SWCNTs [47], which rapidly turns the dispersion gel-like as viscosity increases [47, 48] (Fig. 1(c)). In the traditional sonication procedures, at such high viscosity, sonication becomes ineffective, leading to poor dispersion quality, evidenced by the long and thick branched bundles in Fig. 1(k). Before the gel was formed, we removed the large bundles that are difficult to fully disperse by a mild centrifugation (Fig. S5 in the ESM). Figure 1(l) suggests that the number and size of bundles distinctly decreased after centrifugation and further sonication.

Interestingly, further increasing the sonication time after centrifugation led to the nematic phase with randomly oriented domains. The SWCNT film prepared using SWCNT dispersion at stage V is exhibited in Fig. 1(m). The SWCNT concentration for the isotropic-nematic transition is inversely related to the effective aspect ratio of dispersed SWCNTs. The formation of nematic phase is associated with higher effective aspect ratio [50]. Since the effective aspect ratio is dominated by the degree of dispersion [50], the transition from disordered networks to nematic phase, whether it occurs in dispersion or during the drying process, indicates improved dispersion quality. It further demonstrates the effective delivery of acoustic energy to the bundles using the current method. To observe the dispersion state, the diluted SWCNTs are displayed in Fig. S6 in the ESM. Well-dispersion is achieved, featuring with individualized tubes.

In addition to rheological properties, optical absorption also indicates changes in the dispersion quality and concentration of SWCNTs. We compared the present sonication strategy with sheer mixing and the traditional sonication in Fig. S7 in the ESM. The present method shows no visible agglomerates, unlike traditional methods. Moreover, optical absorption analysis was used to quantitatively evaluate the dispersion efficiency and quality following the method described in the literature [51]. The dispersion efficiency of the present method shows a 30% and 400% improvement compared with the traditional sonication and shear mixing, respectively (details in Supplementary Note 1 and Figs. S7–S10 in the ESM).

3.2 Preparing large-area uniform films with high conductivity

The high-concentration well-dispersed SWCNTs are ideal for conductive films. The high viscosity and distinct shear thinning profiles of high-concentration dispersions help the dispersion spread smoothly under shear force while preventing it from flowing or dewetting during drying. It significantly improves the control over the SWCNT spreading during blade coating (Fig. S1 in the ESM). Thus, large-area uniform films were prepared through scalable doctor blading. An A4-size film with a thickness of approximately 1 μm was prepared within one minute by blade coating, as exhibited in Fig. 2(a). Such films can be prepared on various substrates and readily patterned using masks (Fig. 2(b)).

To maximize electrical conductivity, we employed large-diameter SWCNTs (tuball SWCNT, 1.2–2.0 nm) and doping. Because the mobility of SWCNT is exponentially related to diameter. Moreover, large-diameter semiconducting SWCNTs (1.2–1.7 nm) form ohmic

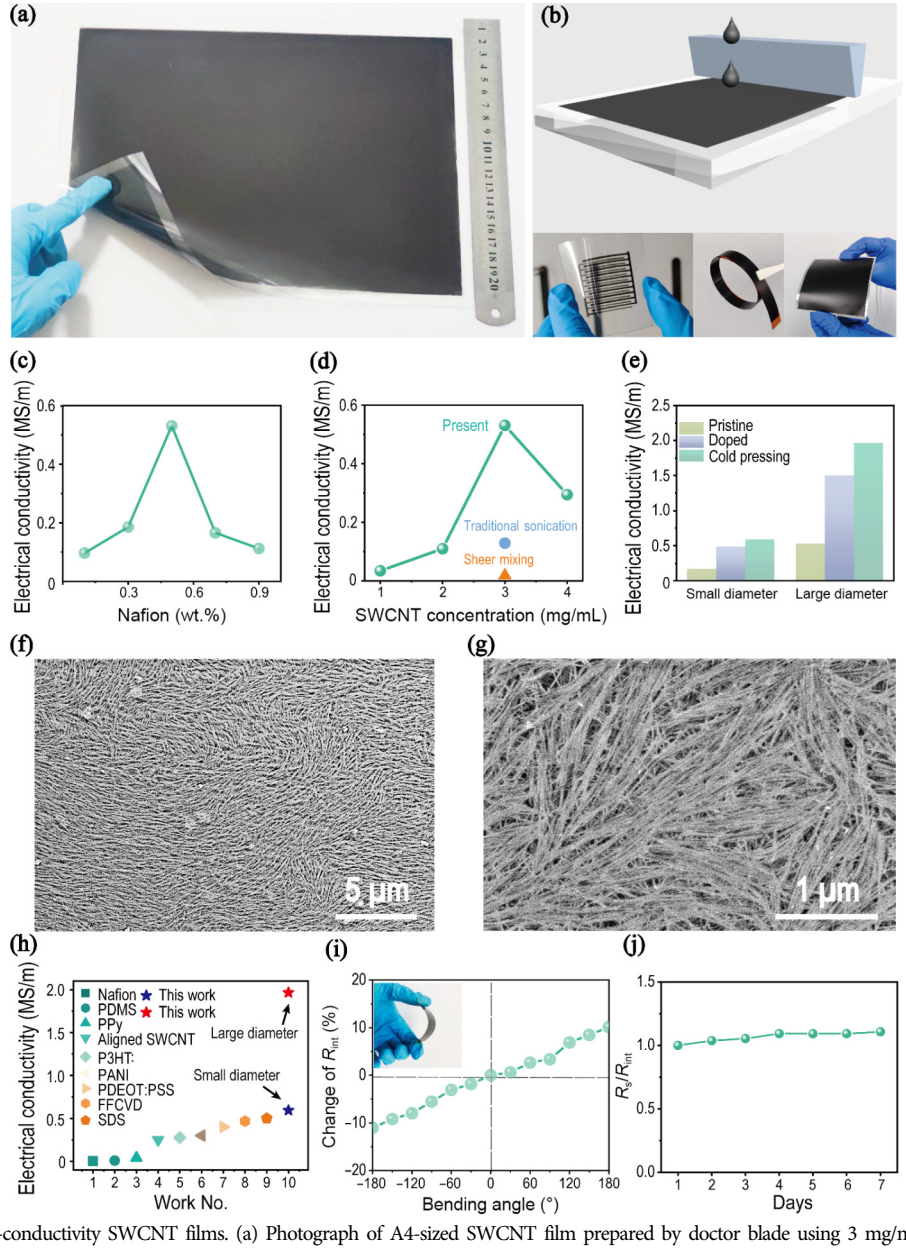

Figure 2 Large-area high-conductivity SWCNT films. (a) Photograph of A4-sized SWCNT film prepared by doctor blade using 3 mg/mL SWCNT dispersion. (b) Schematic diagram of doctor blade. The bottom panel exhibits photographs of patterned SWCNT film and films prepared on stainless steel and tape substrates. (c) Relationship between the conductivity of SWCNT films and concentration of Nafion. The SWCNT concentration was fixed at 3 mg/mL. (d) Relationship between the conductivity of SWCNT films and the SWCNT concentration. The Nafion concentration was fixed at 0.5 wt.%. (e) Electrical conductivity of films after different treatments. (f) and (g) SEM images of large-area SWCNT film prepared from 3 mg/mL SWCNT-Nafion dispersion. (h) Comparison with the polymer-SWCNT or surfactant-SWCNT composite film in literature. The work Nos. 1–9 represent Refs. [34, 44, 35, 59, 3, 54, 6, 40, 62], respectively. (i) The change in film resistance with varying degrees of bending. (j) Variation of sheet resistance of the doped film with time. R_{int} is the initial sheet resistance after doping.

contacts with metal electrodes, facilitating the carrier transport. It makes large-diameter SWCNTs more suitable than small-diameter SWCNTs (0.8–1.0 nm) for high-conductivity films. Thus, we prepared 3 mg/mL large-diameter SWCNT dispersions using the present method. Considering that the mass ratio of polymer and SWCNT is also vital for conductivity, we dispersed 3 mg/mL large-diameter SWCNTs in Nafion at different concentrations and blade-coated them into films (Fig. 2(c)). It suggests that 0.5 wt.% Nafion is the optimal since a lower Nafion concentration cannot effectively disperse 3 mg/mL SWCNTs and a higher Nafion concentration may reduce the conductivity of SWCNT-Nafion (Supplementary Note 2 and Fig. S11 in the ESM). At 0.5 wt.% Nafion, the electrical conductivity increased significantly with the SWCNT concentration and reached 0.53 MS/m at 3 mg/mL, which is nearly 10 times that of 1 mg/mL (Fig. 2(d)). The conductivity of undoped film is even higher than doped polymer-dispersed SWCNTs and conductive polymer-SWCNT composite films in Refs. [3, 52–54]. Such high conductivity was achieved with the Nafion, which has a low intrinsic electron conductivity. Moreover, the conductivity of films prepared by the present method is 4.1 times higher those obtained by traditional sonication, indicating better dispersion quality. However, when the concentration exceeds 3 mg/mL, effective dispersion becomes difficult, leading to a reduced conductivity.

Figure 2(e) shows the impact of the post-treatments on SWCNT

films prepared using 3 mg/mL dispersions. The electrical conductivity of both large-diameter (1.2–2.0 nm) and small-diameter (0.8–1.0 nm) SWCNT films were increased by approximately 3 times after $AuCl_3$ doping (Fig. 2(e)). Specifically, the conductivity of 3 mg/mL large-diameter SWCNT film reached 1.52 MS/m after doping. Although Nafion are reported to dop SWCNTs [55], the doping effect is minor here due to very low Nafion concentration, evidenced by the absence of bleaching in absorption peaks (Fig. S11 in the ESM). It indicates that superior conductivity of the pristine film stems from high dispersion quality, rather than Nafion doping. To further enhance the electrical conductivity, the film was densified by cold press following Liu et al. method [9]. The electrical conductivity of large-diameter SWCNT film increased to 1.97 MS/m (Fig. 2(e)). Liu et al. reported a 12-fold conductivity increase for large-diameter SWCNTs after cold pressing, whereas this work achieved an improvement of 0.45 MS/m, approximately 1.3 times the pre-pressing conductivity (Fig. 2(e)). Although the conductivity increased after densification, the enhancement was less pronounced than that reported in the literature. This is partly due to the high pre-pressing conductivity of 1.52 MS/m in this work, which is even higher than their post-pressing conductivity [9]. It indicates the presence of well-formed conductive pathways and a compact nanotube network before cold pressing. Furthermore, the polymer framework in the film acts as a structural support, limiting compression. As a result, the film thickness decreased by only 200 nm on average after cold pressing, in contrast to the 6 μm reduction observed in dispersant-free films prepared by mold drying, as reported in Ref. [9].

Figure 2(f) and Fig. S12 in the ESM exhibit the nematic SWCNTs in large-area films. The randomly oriented domains distributed across the films. As shown in Fig. 2(g), in each nematic domain, almost all SWCNTs are paralleled aligned with each other, providing numerous straight channels for carrier transport, which reduce the resistance via parallel connections [18]. Different domains are connected by parallel SWCNTs with small-angle bends, forming shared sections. We assume that this morphology works similar to Y-type junctions between individual SWCNTs or thin bundles which benefits the transport of carriers between nanotubes and domains [19, 20, 56]. Compared with Figs. 1(h)–1(i), SWCNTs in Figs. 1(m) and 2(g) are straighter due to nematically induced rigidity [57], facilitating the carrier transport within nanotubes. In addition to the differences in mobility, this is also one of the reasons why the conductivity of large-diameter SWCNTs is significantly higher than that of small-diameter SWCNTs, as depicted in Fig. 2(e). Despite the lack of global alignment, the excellent conductive pathways in Fig. 2(g) contribute to the good connection between different domains across various directions, yielding isotropic high conductivity. This conductivity is the highest reported to date among films prepared from SWCNT dispersions (Fig. 2(h)). Moreover, these domains exhibit characteristics similar to polycrystalline metal films, where conductivity is enhanced under compression during bending and decreased during reverse bending [58]. As shown in Fig. 2(i), bending in different directions results in opposite changes in conductivity. The film conductivity stabilizes within two weeks after doping under ambient conditions (Fig. 2(j)). The variation of conductivity over time is less than 10%.

The uniformity of SWCNT films is another key point for applications. Figure 3 exhibits the film uniformity without cold pressing. High uniformity is achieved after drying rather than relying on cold pressing. As depicted in Figs. 3(a) and 3(b), large-area nematic phase was observed across the SWCNT film, confirming the continuous distribution of densely packed nematic SWCNTs in the film. The conductivity exhibits good uniformity over large areas (Fig. 3(c)). The film shows an average thickness of 1.1 μm with a standard deviation of < 25 nm, indicating that the thickness variation is less than 3% of the average value (Fig. 3(d)). Owing to the polymer matrix filling the voids in the porous SWCNT films, the cross-sectional SEM image reveal a uniform thickness and flat surface, as shown in Fig. 3(e).

Compared with other SWCNT films, the film fabrication process has significant advantages in simplicity. CVD demand precise control over reaction parameters, growth environment, and catalyst distribution, typically involving high temperatures and vacuum conditions [2, 19, 20]. Post-growth treatments, such as superacid treatment [28] and densification [2], further complicate the process. Despite yielding high-performance films, these methods face significant limitations in scalability and yield [19, 23]. Similarly, liquid-phase processing relies on multi-step procedures and precise control over film formation process to achieve high-performance films in recent works. Techniques to achieve alignment [11, 59] and employing superacid [25] introduce additional complexity or enhance the danger. In contrast, by utilizing high-concentration Nafion-SWCNT dispersions, high-performance and large-area films are achieved in a single step through blade coating. The film conductivity was further enhanced to top level among reported liquid-phase film by simply spraying the dopant. Such scalability and performance uniformity are rarely reported, underscoring the broad process window and industrial potential of this approach.

3.3 Thermoelectric performance and large-scale hybrid photovoltaic/thermoelectric system

The TE properties of the SWCNT films prepared under different conditions were investigated (Fig. 4). The power factor reflects the thermal-to-electric conversion efficiency. The Seebeck coefficient denotes the thermal voltage gradient generated by Seebeck effect under a temperature gradient and is related to the derivate of density of states of SWCNTs near the Fermi level. Among the tested raw SWCNTs, CoMoCAT dispersed in Nafion solutions exhibited optimal Seebeck coefficient (Table S1 in the ESM) and was used to fabricate TE devices. 1-μm-thick SWCNT films were prepared by blade-coating using different dispersions. Figure 4(a) illustrates that the dispersion conditions have minimal impact on the Seebeck coefficient, except for a notable drop after doping. The 3 mg/mL sample prepared by shear mixing exhibits the Seebeck coefficient is relatively higher. It coincides with the lowest conductivity in Fig. 4(b), as the Seebeck coefficient is generally inversely related to conductivity. However, for the 3 mg/mL samples prepared by sonication, their Seebeck coefficients remain nearly constant, while the conductivity significantly increases with dispersion quality. Comparing these samples, the Seebeck coefficient and conductivity are decoupled, because the high electrical conductivity is obtained through enhanced dispersion quality other than charge injection. Doping further increases the PF in the 3 mg/mL sample prepared by the present method (Fig. 4(c)). The PF of SWCNT films reached 414.36 and 654.37 $\mu W/(m \cdot K^2)$ before and after doping (Fig. 4(d)). These PF values are compared with the highest PF of polymer-SWCNT films (Fig. 4(d)). Using industrial-scale coating technology, the film area obtained through the single-run coating process in this work significantly exceeds that

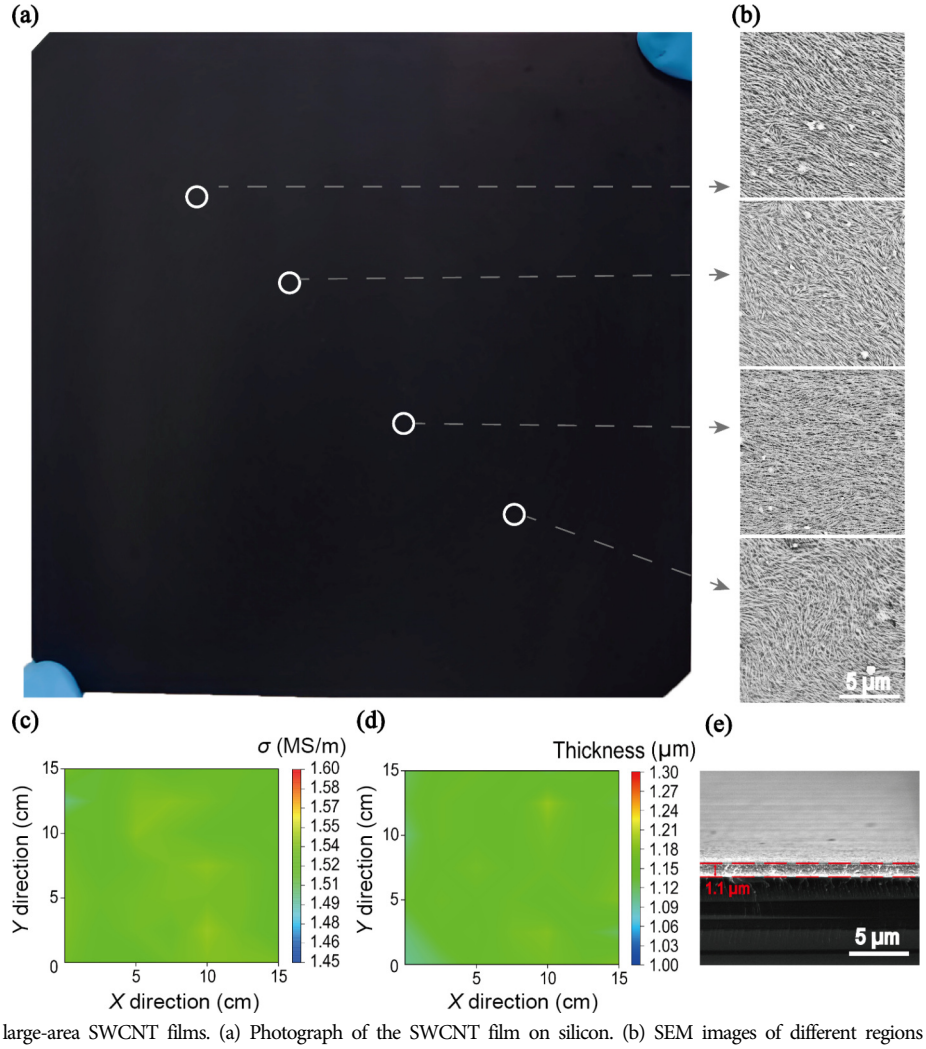

Figure 3 Uniformity of large-area SWCNT films. (a) Photograph of the SWCNT film on silicon. (b) SEM images of different regions of the film. (c) Electrical conductivity map of the corresponding to the film in (a). (d) Thickness distribution of the film in (a). (e) SEM image of cross-section of SWCNT film.

reported in the literature. Considering the significant property differences between different raw SWCNT materials, devices fabricated from the same type of raw SWCNT are generally more comparable. The TE performances are compared with the literature that using CoMoCAT as the raw material (Fig. 4(e)). Although our method did not involve any post-processing purification of CoMoCAT, the TE devices prepared with our simple approach outperform those made from polymer-sorted semiconducting SWCNTs in size and power factor (Table S2 in the ESM).

A flexible TE module where multiple p-type TE films were connected in series was shown in Fig. 4(f). Such small module exhibits power output of 3150 nW and power density (evaluated by dividing the outpower by the cross-sectional area of the thermoelectric devices) of approximately 13.15 W/m^2 at a temperature difference of 60 °C (Fig. 4(f) and Fig. S13 in the ESM).

Our large-area SWCNT films provide a heat management strategy, serving as both TE modules and cooling system for solar cells (Fig. 5(a)). An A4-size film with SWCNT coated on both sides was divided into 56 pieces. The total surface area of these double-sided films is approximately 1200 cm^2 and they were connected to the back of a 330 cm^2 solar cell with copper tape (Fig. 5(a)). The thermoelectric voltage increases with the number of series thermoelectric film elements under varying temperature difference conditions (Fig. 5(b)). The apparent thermal conductivity of our SWCNT film reaches 529 W/(m·K) (Fig. 5(c)), which is even higher than copper (401 W/(m·K)) and similar with that of densified superaligned buckypapers [10]. The high thermal conductivity is closely linked to dispersion quality, as the thermal conductivity of individual nanotubes differs by an order of magnitude from that of bundles. As the SWCNT concentration increases, the density of nanotubes within the film significantly rises, contributing more heat conduction pathways. Additionally, the difference between the apparent thermal conductivity and the in-plane thermal conductivity reported in the literature is attributed to the high specific surface area and emissivity of the 1-μm film [12] (Fig. S14 in the ESM).

To simulate outdoor heating conditions in the laboratory, the cell front was heated to approximately 61 °C under illumination for 10 min, under an ambient temperature of 25 °C with no wind, as depicted in Fig. 5(d). In the PV/TE system, heat is efficiently transferred from the solar cell to the SWCNT film and subsequently to the surface of the film, facilitating heat dissipation. The solar cell temperature reached 53 °C after illuminating for 10 min. The high specific surface area and emissivity of SWCNTs contribute to efficient environmental heat exchange, making the far end of film to approach ambient temperature and resulting in a

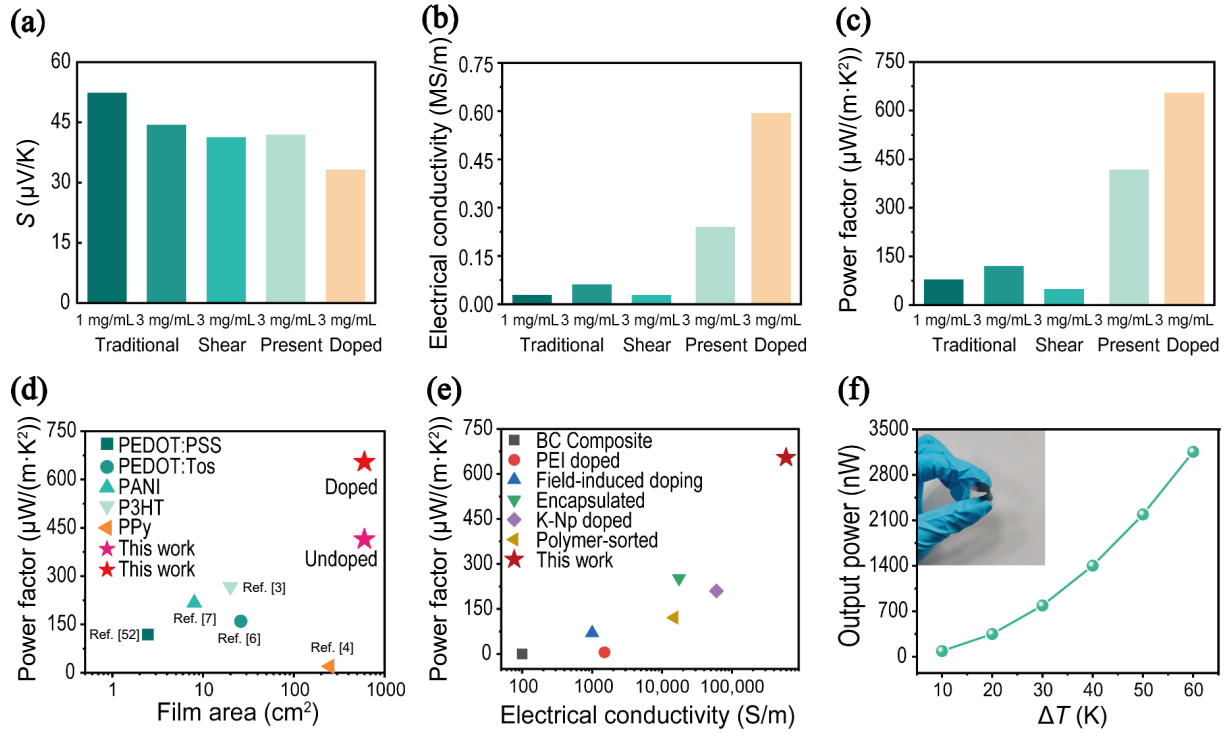

Figure 4 Thermoelectric performance of large-area SWCNT films. (a) Seebeck coefficient of SWCNT films prepared from different dispersions of CoMoCAT SWCNTs. Conduct the test at a controlled temperature of 25 °C. These dispersions were prepared using different dispersion methods. (b) The electronic conductivity of the doped SWCNT films corresponding to (a). (c) The power factors of the doped SWCNT films corresponding to (a). (d) Comparison of the PF values and area of the polymer-SWCNT composite films with those reported in the literature. (e) Comparison with the TE devices fabricated using CoMoCAT SWCNTs. (f) Photograph of a mini thermoelectric module fabricated with the SWCNT film, and relationship between the output power and the temperature difference of the thermoelectric module.

large temperature gradient. In the steady state, the ΔT between two ends of TE film was approximately 30 °C in the in-plane direction, leading to a maximum open-circuit thermal voltage of 70 mV and 3500 nW (Fig. 5(e)). As the temperature increases, the open-circuit voltage of the silicon solar cell decreases markedly, while its current experiences only a marginal increase, leading to a substantial reduction in efficiency. The performance of solar cell with/without TE films is exhibited in Fig. 5(f). The absolute efficiency of the solar cell increases by 0.63% when the temperature decreases from 61 to 53 °C. For example, for a 100 MW PV plants, this enhancement potentially contributes to approximately 3 MW electric power. The high yield of uniform wet-processed SWCNT films enables large-scale integration with standard-sized solar cells. Their lightweight and flexibility grant potentials for rooftop applications. Moreover, the output voltage of SWCNT film is suitable for electrochromic materials, which change color under voltage of 0.2–2 V [60]. The thermoelectric voltage generated by an m^2-scale PV/TE system can drive smart windows, enabling them to regulate indoor sunlight while maintaining high photovoltaic efficiency under intense irradiation.

4 Discussion

While dispersion quality and concentration dominate films' conductivity, the drying process determines the uniformity and scalability. Liu et al. significantly boosted the conductivity by dispersing SWCNTs in ethanol without dispersants followed by cold pressing [9]. They used mold drying to prepare SWCNT films. He et al. achieved high-density aligned films by finely controlling the filtration process [59]. Filtration and mold drying are widely applicable to different dispersion systems because they have a broad tolerance for the rheological properties and drying kinetics of the dispersion. However, these methods are less efficient for producing large-area films. Although substrate modification and precisely controlled evaporation can induce uniform SWCNTs from aqueous dispersions, these films are also limited to laboratory-scale area or low yield [61–63]. Rheological properties and the drying process are critical in industrial film-forming techniques. Even when the SWCNTs are well-dispersed, neglecting these two factors may lead to dewetting and "coffee ring" [29, 30].

The selection of solvent and dispersant determines the rheological properties and the drying process. When it comes to industrial firm-forming techniques, dewetting-induced film shrinkage and defects is a challenge, especially for SWCNT dispersed in aqueous solutions [29]. Besides, "coffee ring" emerges during solvent evaporation further decreasing the uniformity. These non-uniformities are closely related to the properties of the dispersion, making it essential to examine the impact of SWCNT concentration, solvent, and dispersants on the drying process.

The dewetting velocity is $V_{de} = k\gamma\theta^3/\eta$, where k depends on the nature of liquid, γ is the surface tension, θ the contact angle and η the viscosity [29, 64]. When the drying time (t_{dry}) is shorter than the dewetting time $t_{de} = L/V_{de}$ (L is the length scale), rupture and defects are avoided [29, 64, 65]. We compared SWCNT dispersions of varying concentrations in ethanol with Nafion and high-concentration SWCNT dispersion in water with sodium dodecyl sulfate (SDS), a widely used surfactant for SWCNT dispersion. As shown in Fig. 6(a) and Fig. S15 in the ESM, increasing SWCNT content slightly altered hydrophilicity. The contact angles also reflect the wettability relating to the interfacial interactions between

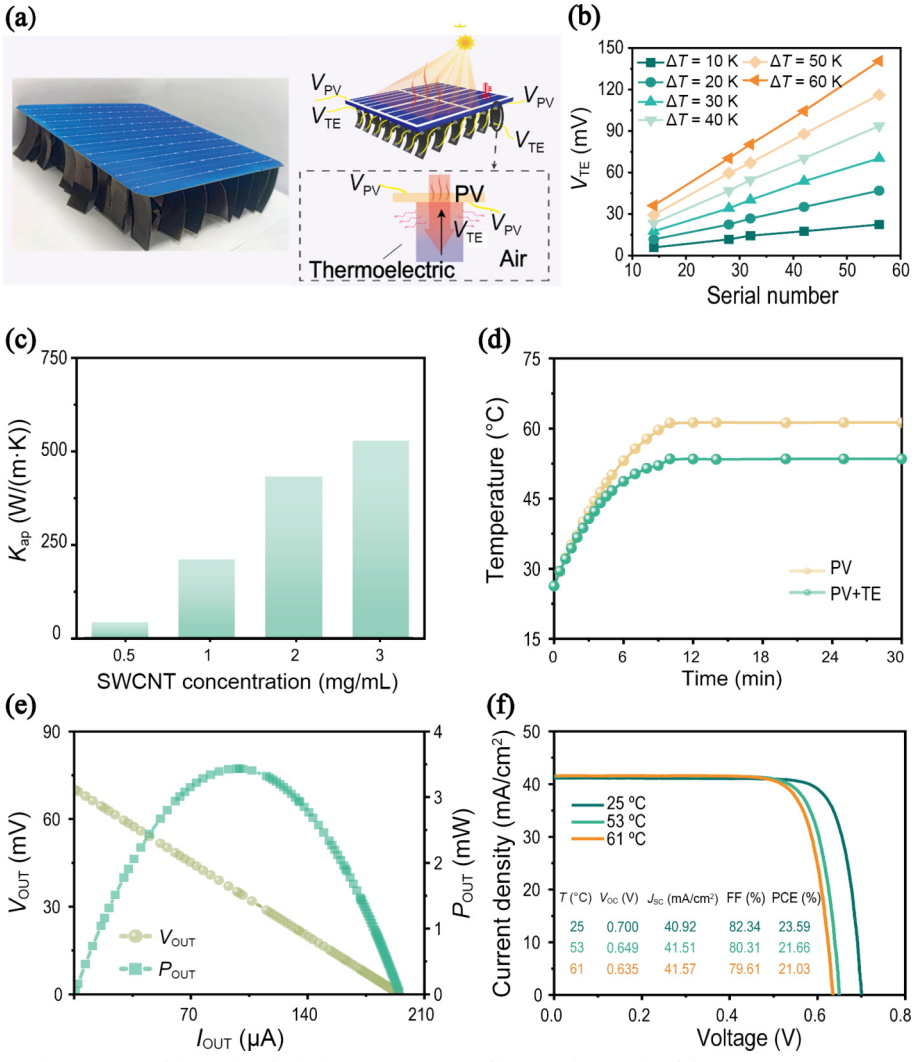

Figure 5 Photovoltaic/thermoelectric system fabricated with the large-area SWCNT film. (a) Photograph of the 330 cm² PV/TE system. The right panel shows a schematic diagram of the PV/TE system. In operation, due to the significant power output difference between the silicon solar cell and the SWCNT TE device, they are connected to external circuits separately rather than in series. (b) The thermal voltage generated by different numbers of serial connections at different temperature differences. (c) Apparent thermal conductivity of SWCNT films prepared using dispersions with different concentrations (d) Variation of the solar cell temperature with illumination time, with/without the backside TE devices. (e) Voltage–current curve and power–current curve of series-connected TE devices on the back of solar cell at a temperature difference of 30 °C between the hot and cold ends. (f) Voltage–current curve of solar cell with/without TE devices on the backside under illumination.

dispersions and the substrates. The increased contact angle with SWCNT concentration indicates less wetting to the substrate and decreased interfacial interactions. This is attributed to the increased viscosity and the hydrophobic nature of SWCNT [66]. However, the variation in contact angle is not significant. And, the contact angle of Nafion-SWCNT dispersion is similar with SDS-SWCNT dispersion at 3 mg/mL. This indicates that the interaction between the dispersion and the hydrophilic glass substrate remains strong. It contributes to a slow V_{de}. The surface tension of Nafion-SWCNT dispersions slightly decreases with increasing SWCNT concentration and remains much lower than that of dispersions in water (Fig. 6(b) and Fig. S16 in the ESM). The low surface tension suppresses the shrinkage of liquid film towards its center during drying, promoting the uniform thickness. Meanwhile, the viscosity of Nafion-SWCNT dispersion increases dramatically with SWCNT concentration (Figs. 1(a) and 1(b) and reaches 10^3 times higher than that of surfactant-dispersed SWCNT dispersion [26]. This significantly extends the dewetting time for Nafion-SWCNT dispersions. And, the dewetting time increased rapidly with SWCNT concentration. By monitoring weight changes of liquid films, we obtained the drying times in 3 mg/mL SWCNT ethanol ($t_{dry,\ ethanol}$) and water ($t_{dry,\ water}$) dispersions. At room temperature, the $t_{dry,\ ethanol}$ is shorter than $t_{dry,\ water}$. In the Nafion-ethanol system, t_{de} increases rapidly with SWCNT concentration, far exceeding the $t_{dry,\ ethanol}$ at concentration above 2 mg/mL, as displayed in Fig. 6(c). As a result, SWCNT can deposit on substrate before film shrinkage and rupture occur.

The self-pining of solute at the contact line between the liquid film and substrate initiate the formation of "coffee rings" [30]. As the solvent evaporates, the compensating flow from the center of the liquid film carries solute to the contact line and accumulates in a dense ring [30]. Therefore, the solute transport, driven by capillary flow, is vital for "coffee ring" formation [30]. In Fig. 6(d), we assessed the diffusion rate of SWCNT in different dispersions (details in Supplementary Note 3). It has been reported that the transport of solutes to the contact line is significantly suppressed

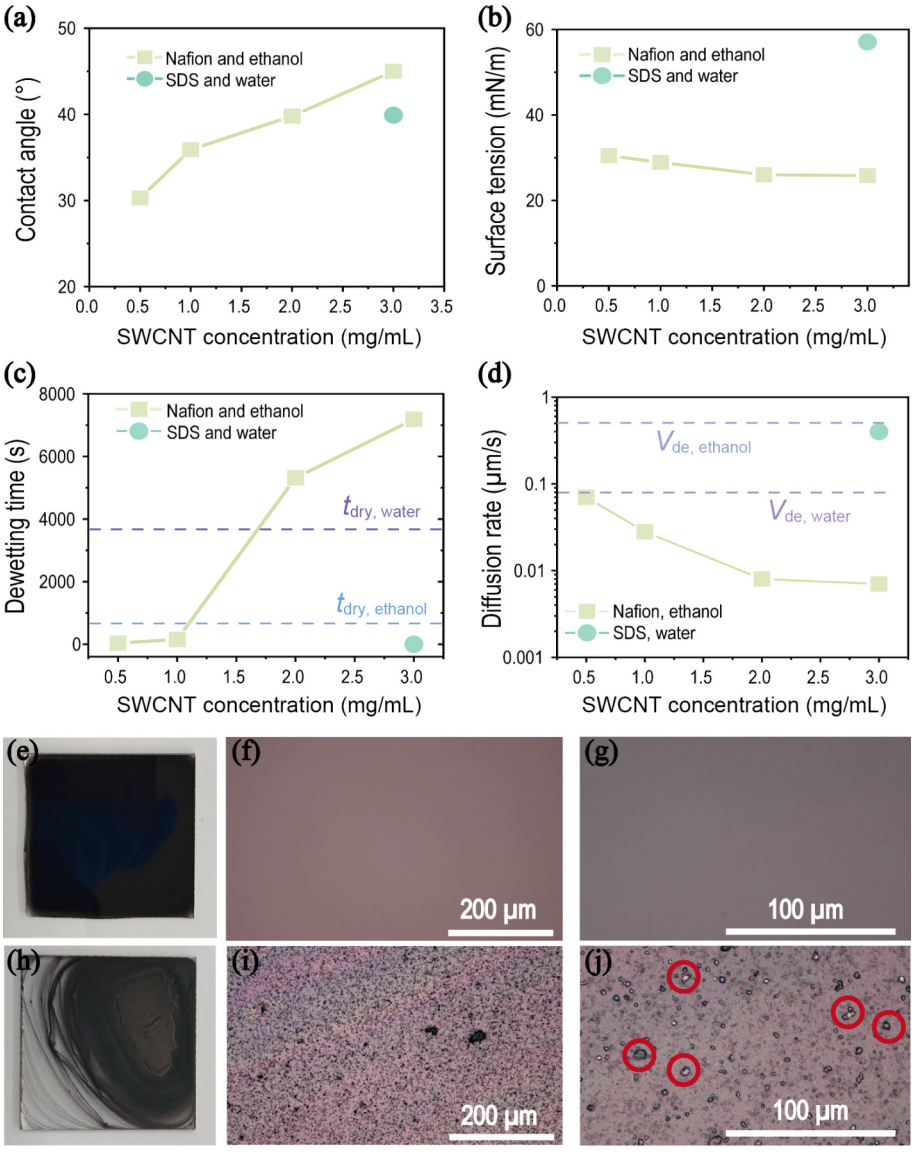

Figure 6 Effect of the drying process on the uniformity of SWCNT films. (a) Contact angles of different SWCNT dispersions on untreated glass. (b) Surface tensions of different SWCNT dispersions. (c) Dewetting times of SWCNT dispersions with different concentration and solvents. (d) Diffusion rates of SWCNTs in various SWCNT dispersions. Notably, the 3 mg/mL sample dispersed in Nafion ethanol solutions in (a)–(d) was prepared by the present sonication method. (e) Photograph of SWCNT film obtained by blade coating the high-concentration SWCNT dispersions prepared by the present dispersion method. (f) and (g) Optical microscopy images of the film in (e). The magnifications of these two images are different. (h) Photograph of SWCNT film obtained by blade coating the surfactant-dispersed high-concentration SWCNT dispersion. (i) and (j) Optical microscopy images of the film in (h). The red circles mark the defects in the film.

when their diffusion rates are remarkably lower than V_{de}, the descending rate of the liquid surface [67]. The high viscosity of high-concentration Nafion-dispersed SWCNT effectively hinders the outward flow of SWCNTs to the contact line and avoid the formation of "coffee ring" [31]. For high-concentration SWCNT in ethanol, their diffusion rates are remarkably lower than the descending rate of liquid film, as shown in Fig. 6(d). Compared with water, ethanol's faster evaporation leads to a much higher $V_{de, ethanol}$ than $V_{de, water}$, where $V_{de, water}$ and $V_{de, ethanol}$ represent the descending rates of water and ethanol surfaces, respectively. It reduces the duration of capillary immersion force that nanotubes experienced. Thus, the formation of "coffee ring" is suppressed by hindering SWCNT long-distance transport to the contact line, further enhancing the uniformity of film.

As a result, the SWCNT film prepared with current dispersions using doctor blade exhibited no "coffee ring" SWCNTs, evidenced by Fig. 6(e). And, the uneven distribution within the film and defects caused by dewetting are not present (Figs. 6(g) and 6(h)) In contrast, the films prepared from aqueous dispersions exhibited distinct "coffee rings" (Fig. 6(h)), along with numerous holes and aggregated SWCNTs in Figs. 6(i) and 6(j).

Furthermore, we hypothesize that the drying process promotes the formation of nematic phases. It has been reported that fully nematic phase emerged at 3.3 mg/mL [68]. So, it is unlikely that fully nematic phase formed within the dispersion. Polarized optical microscopy images confirm the isotropy of the 3 mg/mL SWCNT dispersion prepared by the present method. Upon drop-casting onto a substrate, the solvent evaporation triggered the spontaneous formation of a nematic phase (Fig. S17 in the ESM). The shear force of doctor blade may result in shear alignment [65]. However, the

long-range orientation was not observed in SWCNT films. Meanwhile, we noticed that isotropic nanotubes are distributed beneath the nematic layers, as shown in Fig. 2(g) and Fig. S12 in the ESM. In the liquid film, Nafion readily self-assemble on substrates [69]. And, the SWCNT-Nafion hybrid adheres strongly to the substrate, resisting centrifugal force during spin coating [55]. It indicates strong interaction with substrates. Thus, the bottom-layer SWCNTs preferentially deposit on the substrate along with Nafion and retain their isotropy in the dispersion. The upper nanotubes are concentrated during solvent evaporation, facilitating the isotropy-nematic transition. Due to the very slow diffusion rates of SWCNTs, the concentration occurs across the entire film, leading to a global nematic phases.

5 Conclusion

We established a method for preparing high-concentration, high-dispersion SWCNT solutions in Nafion-ethanol systems, achieving well-dispersed SWCNTs with superior dispersion quality. This method facilitates the scalable fabrication of large-area uniform films with excellent electrical performance, reaching 1.97 MS/m in A4-sized samples. Through improving the dispersion quality, nematic phase emerges in the SWCNT films, benefiting carrier transport. Additionally, the large-area SWCNT films exhibits a thermoelectric power factor of 654.37 μW/(m·K^2) and thermal conductivity of 529 W/(m·K), demonstrating efficient application in the photovoltaic/thermoelectric systems. It offers new insights for advancing SWCNT thermoelectric applications. Investigations on drying process reveal that the high viscosity, fast solvent evaporation and low SWCNT diffusion rates collectively suppressed the dewetting and "coffee ring", which emphasizes the importance of the combination of high-concentration SWCNTs with Nafion and ethanol in achieving superior film uniformity and performance.

Electronic Supplementary Material: Supplementary material (relationship between viscosity and shear rate under different SWCNT concentrations, variation in viscosity with sonication time, schematic diagram of redispersion strategy, relationship between effective acoustic energy delivered to the dispersions and the dispersion temperature, SEM images of sediments of mild centrifugation, SEM images of SWCNTs in stage V after centrifugation, quantitative evaluation of enhanced dispersion efficiency, analysis on the dispersion quality and efficiency, the influence of dispersion volume and centrifugation speed on dispersion quality, relationship between well-dispersed SWCNT concentrations and effective acoustic energy delivered to the dispersions, analysis on the doping state and dispersion quality of SWCNTs at varying Nafion concentrations using optical absorption spectra, variations in optical absorption of SWCNTs dispersed with different concentrations of Nafion, the oriented domains in different regions of the large-area film, the Seebeck coefficients of different raw SWCNTs dispersed by various dispersants, TE performances of SWCNT films using CoMoCAT SWCNTs as raw materials, performance of the mini TE module in Fig. 5(e), in-plane thermal conductivity of SWCNT films prepared using different dispersions, contact angles of different SWCNT dispersions on untreated glass, surface tension assessment of different dispersions using pendent drop apparatus, diffusion rate of SWCNTs in the dispersion, and cross polarized microscopy images of SWCNT film and SWCNT dispersion) is available in the online version of this article at https://doi.org/10.26599/NR.2025.94907383.

Data availability

All data needed to support the conclusions in the paper are presented in the manuscript and the Electronic Supplementary Material. Additional data related to this paper may be requested from the corresponding author upon request.

Acknowledgements

This work was financially supported by the National Natural Science Foundation of China (Nos. 52402048 and 62274054), the "333 project" of Hebei Province (No. C20221014), Hebei Provincial Innovation Capability Enhancement Program Project (No. 24464302D), Hebei University President's Research Fund (No. XZJJ202201), Natural Science Foundation of Hebei Province (Nos. F2023201001 and F2023201005), Interdisciplinary research project of Hebei University (No. DXK202303), the Central Guidance on Local Science and Technology Development Fund Project of Hebei Province (Nos. 236Z4307G and 226Z4306G), Hebei province Science Foundation for Distinguished Young Scholars (No. F2021201035), and S&T Program of Hebei (No. 242Q4501Z).

Declaration of competing interest

All the contributing authors report no conflict of interests in this work.

Author contribution statement

X. Y. Y.: Data curation, validation, writing manuscript, experimental design. D. H. Y.: Project administration, funding acquisition, data curation, experimental design, writing manuscript. X. F. Y.: Validation. X. C.: Validation. D. H. Z.: Validation. A. A. W.: Experimental design. Y. M. X.: Validation. X. L. Y.: Validation. J. X. C.: Data curation. X. J. L.: Data curation. S. M.: Data curation. Q. G.: Data curation, validation, experimental design. S. F. W.: Data curation. H. P. L.: Experimental design, validation. J. H. C.: Funding acquisition, experimental design, project administration. All the authors have approved the final manuscript.

Use of AI statement

None.

References

[1] Lijima, S.; Ichihashi, T. Single-shell carbon nanotubes of 1-nm diameter. *Nature* **1993**, *363*, 603–605.

[2] Wang, H.; Sun, X.; Wang, Y. Z.; Li, K. C.; Wang, J.; Dai, X.; Chen, B.; Chong, D. T.; Zhang, L. Y.; Yan, J. J. Acid enhanced zipping effect to densify MWCNT packing for multifunctional MWCNT films with ultra-high electrical conductivity. *Nat. Commun.* **2023**, *14*, 380.

[3] Hong, C. T.; Lee, W.; Kang, Y. H.; Yoo, Y.; Ryu, J.; Cho, S. Y.; Jang, K. S. Effective doping by spin-coating and enhanced thermoelectric power factors in SWCNT/P3HT hybrid films. *J. Mater. Chem. A* **2015**, *3*, 12314–12319.

[4] Liang, L. R.; Gao, C. Y.; Chen, G. M.; Guo, C. Y. Large-area, stretchable, super flexible and mechanically stable thermoelectric films of polymer/carbon nanotube composites. *J. Mater. Chem. C* **2016**, *4*, 526–532.

[5] Yao, Q.; Chen, L. D.; Zhang, W. Q.; Liufu, S. C.; Chen, X. H. Enhanced thermoelectric performance of single-walled carbon nanotubes/polyaniline hybrid nanocomposites. *ACS Nano* **2010**, *4*, 2445–2451.
[6] Liang, L. R.; Wang, X. D.; Wang, M. M.; Liu, Z. X.; Chen, G. M.; Sun, G. X. Flexible poly(3,4-ethylenedioxythiophene)-tosylate/SWCNT composite films with ultrahigh electrical conductivity for thermoelectric energy harvesting. *Compos. Commun.* **2021**, *25*, 100701.
[7] Avery, A. D.; Zhou, B. H.; Lee, J.; Lee, E. S.; Miller, E. M.; Ihly, R.; Wesenberg, D.; Mistry, K. S.; Guillot, S. L.; Zink, B. L. et al. Tailored semiconducting carbon nanotube networks with enhanced thermoelectric properties. *Nat. Energy* **2016**, *1*, 16033.
[8] Blackburn, J. L.; Ferguson, A. J.; Cho, C.; Grunlan, J. C. Carbon-nanotube-based thermoelectric materials and devices. *Adv. Mater.* **2018**, *30*, 1704386.
[9] Liu, Y. M.; Shi, X. L.; Wu, T.; Wu, H.; Mao, Y. Q.; Cao, T. Y.; Wang, D. Z.; Liu, W. D.; Li, M.; Liu, Q. F. et al. Boosting thermoelectric performance of single-walled carbon nanotubes-based films through rational triple treatments. *Nat. Commun.* **2024**, *15*, 3426.
[10] Zhang, L.; Zhang, G.; Liu, C. H.; Fan, S. S. High-density carbon nanotube buckypapers with superior transport and mechanical properties. *Nano Lett.* **2012**, *12*, 4848–4852.
[11] Zeng, Z. H.; Wang, G.; Wolan, B. F.; Wu, N.; Wang, C. X.; Zhao, S. Y.; Yue, S. Y.; Li, B.; He, W. D.; Liu, J. R. et al. Printable aligned single-walled carbon nanotube film with outstanding thermal conductivity and electromagnetic interference shielding performance. *Nano-Micro Lett.* **2022**, *14*, 179.
[12] Zhou, W. B.; Fan, Q. X.; Zhang, Q.; Li, K. W.; Cai, L.; Gu, X. G.; Yang, F.; Zhang, N.; Xiao, Z. J.; Chen, H. L. et al. Ultrahigh-power-factor carbon nanotubes and an ingenious strategy for thermoelectric performance evaluation. *Small* **2016**, *12*, 3407–3414.
[13] Green, M. A.; Bremner, S. P. Energy conversion approaches and materials for high-efficiency photovoltaics. *Nat. Mater.* **2017**, *16*, 23–34.
[14] Jošt, M.; Lipovšek, B.; Glažar, B.; Al-Ashouri, A.; Brecl, K.; Matič, G.; Magomedov, A.; Getautis, V.; Topič, M.; Albrecht, S. Perovskite solar cells go outdoors: Field testing and temperature effects on energy yield. *Adv. Energy Mater.* **2020**, *10*, 2000454.
[15] Shittu, S.; Li, G. Q.; Akhlaghi, Y. G.; Ma, X. L.; Zhao, X. D.; Ayodele, E. Advancements in thermoelectric generators for enhanced hybrid photovoltaic system performance. *Renew. Sustain. Energy Rev.* **2019**, *109*, 24–54.
[16] Hou, P. X.; Zhang, F.; Zhang, L. L.; Liu, C.; Cheng, H. M. Synthesis of carbon nanotubes by floating catalyst chemical vapor deposition and their applications. *Adv. Funct. Mater.* **2022**, *32*, 2108541.
[17] Wu, Y. Z.; Zhao, X. W.; Shang, Y. Y.; Chang, S. L.; Dai, L. X.; Cao, A. Y. Application-driven carbon nanotube functional materials. *ACS Nano* **2021**, *15*, 7946–7974.
[18] Ilatovskii, D. A.; Gilshtein, E. P.; Glukhova, O. E.; Nasibulin, A. G. Transparent conducting films based on carbon nanotubes: Rational design toward the theoretical limit. *Adv. Sci.* **2022**, *9*, 2201673.
[19] Zhang, Q.; Zhou, W. Y.; Xia, X. G.; Li, K. W.; Zhang, N.; Wang, Y. C.; Xiao, Z. J.; Fan, Q. X.; Kauppinen, E. I.; Xie, S. S. Transparent and freestanding single-walled carbon nanotube films synthesized directly and continuously via a blown aerosol technique. *Adv. Mater.* **2020**, *32*, 2004277.
[20] Yue, Y.; Zhang, D.; Wang, P. Y.; Xia, X. G.; Wu, X.; Zhang, Y. J.; Mei, J.; Li, S. Q.; Li, M. M.; Wang, Y. C. et al. Large-area flexible carbon nanofilms with synergistically enhanced transmittance and conductivity prepared by reorganizing single-walled carbon nanotube networks. *Adv. Mater.* **2024**, *36*, 2313971.
[21] Hecht, D. S.; Thomas, D.; Hu, L. B.; Ladous, C.; Lam, T.; Park, Y.; Irvin, G.; Drzaic, P. Carbon-nanotube film on plastic as transparent electrode for resistive touch screens. *J. Soc. Inf. Display* **2009**, *17*, 941–946.
[22] Jiang, S.; Hou, P. X.; Chen, M. L.; Wang, B. W.; Sun, D. M.; Tang, D. M.; Jin, Q.; Guo, Q. X.; Zhang, D. D.; Du, J. H. et al. Ultrahigh-performance transparent conductive films of carbon-welded isolated single-wall carbon nanotubes. *Sci. Adv.* **2018**, *4*, eaap9264.
[23] Zhang, Q.; Nam, J. S.; Han, J. Y.; Datta, S.; Wei, N.; Ding, E. X.; Hussain, A.; Ahmad, S.; Skakalova, V.; Khan, A. T. et al. Large-diameter carbon nanotube transparent conductor overcoming performance-yield tradeoff. *Adv. Funct. Mater.* **2022**, *32*, 2103397.
[24] Nirmalraj, P. N.; Lyons, P. E.; De, S.; Coleman, J. N.; Boland, J. J. Electrical connectivity in single-walled carbon nanotube networks. *Nano Lett.* **2009**, *9*, 3890–3895.
[25] Headrick, R. J.; Williams, S. M.; Owens, C. E.; Taylor, L. W.; Dewey, O. S.; Ginestra, C. J.; Liberman, L.; Ya'akobi, A. M.; Talmon, Y.; Maruyama, B. et al. Versatile acid solvents for pristine carbon nanotube assembly. *Sci. Adv.* **2022**, *8*, eabm3285.
[26] Yang, D. H.; Li, L. H.; Li, X.; Xi, W.; Zhang, Y. J.; Liu, Y. M.; Wei, X. J.; Zhou, W. Y.; Wei, F.; Xie, S. S. et al. Preparing high-concentration individualized carbon nanotubes for industrial separation of multiple single-chirality species. *Nat. Commun.* **2023**, *14*, 2491.
[27] Canselier, J. P.; Delmas, H.; Wilhelm, A. M.; Abismaïl, B. Ultrasound emulsification—An overview. *J. Dispers. Sci. Technol.* **2002**, *23*, 333–349.
[28] Zhang, X.; De Volder, M.; Zhou, W. B.; Issman, L.; Wei, X. J.; Kaniyoor, A.; Terrones Portas, J.; Smail, F.; Wang, Z. B.; Wang, Y. C. et al. Simultaneously enhanced tenacity, rupture work, and thermal conductivity of carbon nanotube fibers by raising effective tube portion. *Sci. Adv.* **2022**, *8*, eabq3515.
[29] Dan, B.; Irvin, G. C.; Pasquali, M. Continuous and scalable fabrication of transparent conducting carbon nanotube films. *ACS Nano* **2009**, *3*, 835–843.
[30] Deegan, R. D.; Bakajin, O.; Dupont, T. F.; Huber, G.; Nagel, S. R.; Witten, T. A. Capillary flow as the cause of ring stains from dried liquid drops. *Nature* **1997**, *389*, 827–829.
[31] Cui, L. Y.; Zhang, J. H.; Zhang, X. M.; Huang, L.; Wang, Z. H.; Li, Y. F.; Gao, H. N.; Zhu, S. J.; Wang, T. Q.; Yang, B. Suppression of the coffee ring effect by hydrosoluble polymer additives. *ACS Appl. Mater. Interfaces* **2012**, *4*, 2775–2780.
[32] Mukherjee, R.; Sharma, A. Instability, self-organization and pattern formation in thin soft films. *Soft Matter* **2015**, *11*, 8717–8740.
[33] Bulmer, J. S.; Kaniyoor, A.; Elliott, J. A. A meta-analysis of conductive and strong carbon nanotube materials. *Adv. Mater.* **2021**, *33*, 2008432.
[34] Choi, Y.; Kim, Y.; Park, S. G.; Kim, Y. G.; Sung, B. J.; Jang, S. Y.; Kim, W. Effect of the carbon nanotube type on the thermoelectric properties of CNT/Nafion nanocomposites. *Org. Electron.* **2011**, *12*, 2120–2125.
[35] Wang, L. M.; Yao, Q.; Xiao, J. X.; Zeng, K. Y.; Qu, S. Y.; Shi, W.;Wang, Q.; Chen, L. D. Engineered molecular chain ordering in singlewalled carbon nanotubes/polyaniline composite films for highperformance organic thermoelectric materials. *Chem. Asian J.* **2016**, *11*, 1804–1810.
[36] Meng, C.; Liu, C.; Fan, S. A. Promising approach to enhanced thermoelectric properties using carbon nanotube networks. *Adv. Mater.* **2010**, *22*, 535–539.
[37] Wang, Y. Z.; Li, Q.; Wang, J.; Li, Z. C.; Li, K. C.; Dai, X.; Pan, J. H.; Wang, H. Understanding the solvent effects on polarity switching and thermoelectric properties changing of solution-processable n-type single-walled carbon nanotube films. *Nano Energy* **2022**, *93*, 106804.
[38] Luo, C.; Zuo, X. L.; Wang, L.; Wang, E. G.; Song, S. P.; Wang, J.; Wang, J.; Fan, C. H.; Cao, Y. Flexible carbon nanotube-polymer composite films with high conductivity and superhydrophobicity made by solution process. *Nano Lett.* **2008**, *8*, 4454–4458.
[39] Xi, W.; Xia, X. G.; Zhu, J. C.; Yang, D. H.; Xie, S. S. Enhancing

electrochemical capacity and interfacial stability of lithium-ion batteries through side reaction modulation with ultrathin carbon nanotube film and optimized lithium cobalt oxide particle size. *Nano Res.* **2024**, *17*, 7230–7241.

[40] Zhou, W. B.; Fan, Q. X.; Zhang, Q.; Cai, L.; Li, K. W.; Gu, X. G.; Yang, F.; Zhang, N.; Wang, Y. C.; Liu, H. P. et al. High-performance and compact-designed flexible thermoelectric modules enabled by a reticulate carbon nanotube architecture. *Nat. Commun.* **2017**, *8*, 14886.

[41] Jiao, X. Y.; Xu, L. L.; Sun, X. Y.; Shi, C.; Hou, P. X.; Liu, C.; Cheng, H. M. Single-wall carbon nanotube fiber non-woven fabrics with a high electrothermal heating response. *Nano Res.* **2024**, *17*, 5621–5628.

[42] Wang, J.; Musameh, M.; Lin, Y. H. Solubilization of carbon nanotubes by Nafion toward the preparation of amperometric biosensors. *J. Am. Chem. Soc.* **2003**, *125*, 2408–2409.

[43] Gao, C. Q.; Guo, M. Y.; Liu, Y. K.; Zhang, D. Y.; Gao, F.; Sun, L.; Li, J. S.; Chen, X. C.; Terrones, M.; Wang, Y. Q. Surface modification methods and mechanisms in carbon nanotubes dispersion. *Carbon* **2023**, *212*, 118133.

[44] Prabhakar, R.; Hossain, S.; Zheng, W.; Athikam, P. K.; Zhang, Y.; Hsieh, Y. Y.; Skafidas, E.; Wu, Y.; Shanov, V.; Bahk, J. H. Tunneling-limited thermoelectric transport in carbon nanotube networks embedded in poly(dimethylsiloxane) elastomer. *ACS Appl. Energy Mater.* **2019**, *2*, 2419–2426.

[45] Zhu, J.; Shim, B. S.; Di Prima, M.; Kotov, N. A. Transparent conductors from carbon nanotubes LBL-assembled with polymer dopant with π-π electron transfer. *J. Am. Chem. Soc.* **2011**, *133*, 7450–7460.

[46] Huang, Y. Y.; Terentjev, E. M. Dispersion and rheology of carbon nanotubes in polymers. *Int. J. Mater. Form.* **2008**, *1*, 63–74.

[47] Lee, H. W.; You, W.; Barman, S.; Hellstrom, S.; LeMieux, M. C.; Oh, J. H.; Liu, S. H.; Fujiwara, T.; Wang, W. M.; Chen, B. et al. Lyotropic liquid-crystalline solutions of high-concentration dispersions of single-walled carbon nanotubes with conjugated polymers. *Small* **2009**, *5*, 1019–1024.

[48] Huang, Y. Y.; Ahir, S. V.; Terentjev, E. M. Dispersion rheology of carbon nanotubes in a polymer matrix. *Phys. Rev. B* **2006**, *73*, 125422.

[49] Dumée, L.; Sears, K.; Schütz, J.; Finn, N.; Duke, M.; Gray, S. Influence of the sonication temperature on the debundling kinetics of carbon nanotubes in propan-2-ol. *Nanomaterials* **2013**, *3*, 70–85.

[50] Chatterjee, T.; Krishnamoorti, R. Rheology of polymercarbon nanotubes composites. *Soft Matter* **2013**, *9*, 9515–9529.

[51] Keinänen, P.; Siljander, S.; Koivula, M.; Sethi, J.; Sarlin, E.; Vuorinen, J.; Kanerva, M. Optimized dispersion quality of aqueous carbon nanotube colloids as a function of sonochemical yield and surfactant/CNT ratio. *Heliyon* **2018**, *4*, e00787.

[52] Yu, C.; Choi, K.; Yin, L.; Grunlan, J. C. Light-weight flexible carbon nanotube based organic composites with large thermoelectric power factors. *ACS Nano* **2011**, *5*, 7885–7892.

[53] Wei, S. S.; Huang, X.; Deng, L.; Yan, Z. C.; Chen, G. M. Facile preparations of layer-like and honeycomb-like films of poly(3,4-ethylenedioxythiophene)/carbon nanotube composites for thermoelectric application. *Compos. Sci. Technol.* **2021**, *208*, 108759.

[54] Li, H.; Liu, Y. L.; Li, P. C.; Liu, S. Q.; Du, F. P.; He, C. B. Enhanced thermoelectric performance of carbon nanotubes/polyaniline composites by multiple interface engineering. *ACS Appl. Mater. Interfaces* **2021**, *13*, 6650–6658.

[55] Chen, J. H.; Wan, L.; Li, H.; Yan, J.; Ma, J. K.; Sun, B.; Li, F.; Flavel, B. S. A polymer/carbon-nanotube ink as a boron-dopant/inorganic-passivation free carrier selective contact for silicon solar cells with over 21% efficiency. *Adv. Funct. Mater.* **2020**, *30*, 2004476.

[56] Sun, D. M.; Timmermans, M. Y.; Tian, Y.; Nasibulin, A. G.; Kauppinen, E. I.; Kishimoto, S.; Mizutani, T.; Ohno, Y. Flexible high-performance carbon nanotube integrated circuits. *Nat. Nanotechnol.* **2011**, *6*, 156–161.

[57] Vroege, G. J.; Odijk, T. Induced chain rigidity, splay modulus and other properties of nematic polymer liquid crystals. *Macromolecules* **1988**, *21*, 2848–2858.

[58] Yang, C.; Souchay, D.; Kneiß, M.; Bogner, M.; Wei, H. M.; Lorenz, M.; Oeckler, O.; Benstetter, G.; Fu, Y. Q.; Grundmann, M. Transparent flexible thermoelectric material based on non-toxic earth-abundant p-type copper iodide thin film. *Nat. Commun.* **2017**, *8*, 16076.

[59] He, X. W.; Gao, W. L.; Xie, L. J.; Li, B.; Zhang, Q.; Lei, S. D.; Robinson, J. M.; Hároz, E. H.; Doorn, S. K.; Wang, W. P. et al. Wafer-scale monodomain films of spontaneously aligned single-walled carbon nanotubes. *Nat. Nanotechnol.* **2016**, *11*, 633–638.

[60] Gu, C.; Jia, A. B.; Zhang, Y. M.; Zhang, S. X. A. Emerging electrochromic materials and devices for future displays. *Chem. Rev.* **2022**, *122*, 14679–14721.

[61] Su, W.; Yang, D. H.; Cui, J. M.; Wang, F. T.; Wei, X. J.; Zhou, W. Y.; Kataura, H.; Xie, S. S.; Liu, H. P. Ultrafast wafer-scale assembly of uniform and highly dense semiconducting carbon nanotube films for optoelectronics. *Carbon* **2020**, *163*, 370–378.

[62] Geng, H. Z.; Kim, K. K.; So, K. P.; Lee, Y. S.; Chang, Y.; Lee, Y. H. Effect of acid treatment on carbon nanotube-based flexible transparent conducting films. *J. Am. Chem. Soc.* **2007**, *129*, 7758–7759.

[63] Engel, M.; Small, J. P.; Steiner, M.; Freitag, M.; Green, A. A.; Hersam, M. C.; Avouris, P. Thin film nanotube transistors based on self-assembled, aligned, semiconducting carbon nanotube arrays. *ACS Nano* **2008**, *2*, 2445–2452.

[64] Redon, C.; Brochard-Wyart, F.; Rondelez, F. Dynamics of dewetting. *Phys. Rev. Lett.* **1991**, *66*, 715–718.

[65] Akbari, A.; Sheath, P.; Martin, S. T.; Shinde, D. B.; Shaibani, M.; Banerjee, P. C.; Tkacz, R.; Bhattacharyya, D.; Majumder, M. Large-area graphene-based nanofiltration membranes by shear alignment of discotic nematic liquid crystals of graphene oxide. *Nat. Commun.* **2016**, *7*, 10891.

[66] Zitzenbacher, G.; Dirnberger, H.; Längauer, M.; Holzer, C. Calculation of the contact angle of polymer melts on tool surfaces from viscosity parameters. *Polymers* **2017**, *10*, 38.

[67] Li, Y. A.; Yang, Q.; Li, M. Z.; Song, Y. L. Rate-dependent interface capture beyond the coffee-ring effect. *Sci. Rep.* **2016**, *6*, 24628.

[68] Kojima, K.; Aizawa, M.; Yamamoto, T.; Muroga, S.; Kobashi, K.; Okazaki, T. Liquid crystalline behaviors of single-walled carbon nanotubes in an aqueous sodium cholate dispersion. *Langmuir* **2022**, *38*, 8899–8905.

[69] Paul, D. K.; Karan, K.; Docoslis, A.; Giorgi, J. B.; Pearce, J. Characteristics of self-assembled ultrathin Nafion films. *Macromolecules* **2013**, *46*, 3461–3475.